Edgar A. Estupiñan
eep@mek.dtu.dk

Ilmar F. Santos
Senior Member, ABCM
ifs@mek.dtu.dk
Technical University of Denmark
Department of Mechanical Engineering
Nils Koppels Allé, Building 404, DK-2800
Kgs. Lyngby, Denmark

Modelling Hermetic Compressors Using Different Constraint Equations to Accommodate Multibody Dynamics and Hydrodynamic Lubrication

In this work, the steps involved for the modelling of a reciprocating linear compressor are described in detail. The dynamics of the mechanical components are described with the help of multibody dynamics (rigid components) and finite elements method (flexible components). Some of the mechanical elements are supported by fluid film bearings, where the hydrodynamic interaction forces are described by the Reynolds equation. The system of nonlinear equations is numerically solved for three different restrictive conditions of the motion of the crank, where the third case takes into account lateral and tilting oscillations of the extremity of the crankshaft. The numerical results of the behaviour of the journal bearings for each case are presented giving some insights into design parameters such as, maximum oil film pressure, minimum oil film thickness, maximum vibration levels and dynamic reaction forces among machine components, looking for the optimization and application of active lubrication towards vibration reduction.
Keywords*: hermetic compressor, multibody dynamics, journal bearing, Reynolds equation, hydrodynamic lubrication.*

Introduction

One of the most common types of compressors used in the refrigeration field is the piston compressor, also known as reciprocating compressor. Small-scale hermetic reciprocating compressors are widely used to compress coolant gas in household refrigerators and air-conditioners. It was at the beginning of the Sixties when these small machines became a household appliance of common use in the industrialized countries. Since then, numerous research studies have been carried out in order to optimize the design and to improve the thermal and mechanical efficiency of refrigeration compressors. Positive displacement compressors mechanically drive the refrigerant gas from the evaporator at low-pressure side to the condenser at high-pressure side, reducing the compressor chamber volume. Reciprocating compressors use pistons that are driven directly through a slider-crank mechanism, converting the rotating movement of the rotor to an oscillating motion. A hermetic reciprocating compressor is a particular case where motor and compressor are directly coupled on the same shaft and contained within the same housing (welded steel shell) and in contact with the refrigerant and oil (Rigola, 2002). A picture and a schematic draw of a hermetic reciprocating compressor used in household refrigerators are shown in Fig.1.

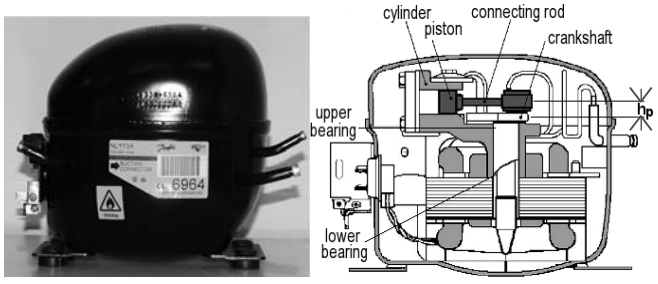

Figure 1. Picture and schematic draw of a hermetic reciprocating compressor.

The study and optimization of the dynamic behaviour of reciprocating compressors, taking in account the hydrodynamics of bearings, are of significant importance for the development of new prototypes. The performance of the bearings affects key functions such as durability and noise and vibration behaviour of the compressor. Optimization studies of the performance of journal bearings by means of numerical simulation may reduce development costs for prototype testing work significantly. Several studies that involve numerical studies and computational models for the analysis of small reciprocating compressors are found in the literature, as it can be seen in the works carried out by Rasmussen (1997) and Rigola (2002). In some studies, numerical simulations of the refrigerant flow through the valves and inside the cylinder during the compression cycle have been included (Longo and Gasparella, 2003), whereas in others the focus has been on the dynamics of motion in steady and transient conditions (Dufour, *et al*., 1995). Some researchers have included the coupling of fluid-structure dynamics in order to particularly analyse the dynamics of the piston (Gommed and Etsion, 1993; Cho and Moon, 2005). In a study carried out by Kim and Han (2004), an analytical model of the coupled dynamic behaviour of the piston and crankshaft was developed and comparisons between a finite bearing model and a short bearing approach were included. In the same study, a numerical procedure that combines Newton-Raphson method and the successive over relaxation scheme was also presented. In the study carried out by Cho and Moon (2005), a time-incremental numerical algorithm to solve a finite differences model for the estimation of the oil film pressure was coupled with a finite element model for the computation of the structural deformation of the piston. As it is described here, many of the research studies related to compressor modelling are mainly focused on the study of the thermal and fluid dynamic behaviour. In contrast, the main focus of the present work is on the developing of a multibody dynamic model of a hermetic compressor, where the dynamics of the fluid film bearings and the flexibility of the crankshaft are included. The multibody dynamic model, which includes the main mechanical components of the hermetic compressor, is coupled with a finite elements model of the rotor and the hydrodynamic interaction forces, which are computed using analytical solutions of the Reynolds equation. The influence of the crankshaft tilting oscillations on design parameters, such as the minimum film

Paper accepted December, 2008. Technical Editor: Domingos A. Rade.

thickness and maximum pressures are carefully investigated, since the finite element model allows capturing of such movements. The elasto-hydrodynamic theory, which takes in account the bearing and housing flexibility, is not considered in this work, since it is presented only in very special cases.

Nomenclature

A_p =transversal area of the piston, m^2
c_b =radial clearance of the bearing, m
D_p =piston diameter, m
e_c =mass eccentricity of the crank, m
f =vector of forces, N
$\mathbf{f}_b$ =vector of journal bearing forces, N
h_b =oil film thickness, m
h_p =length of crank pin, m
I =moment of inertia tensor
l =length of the connecting rod, m
l_b =width of the bearing, m
m =mass, kg
ndof =number of degrees of freedom
P_g =gas pressure inside the cylinder, Pa
p =fluid film pressure, Pa
rpm =revolutions per minute
r =radius, m
S =Sommerfeld number
T_i =transformation matrix in the coordinate i
x_B =piston position along the X direction, m

Greek Symbols

Ω =rotational speed of the crankshaft, rad/s
θ =rotation angle of the crank around Z-Z axis, rad
α =rotation angle of the connecting rod, rad
β =rotation angle around X-X axis, rad
Γ =rotation angle around Y1-Y1 axis, rad
μ =viscosity oil film, Pa.s
ε =eccentricity ratio
ϕ =attitude angle, rad
τ_z =motor shaft torque, Nm

Subscripts

A,B,C =relative to the points A, B or C, respectively
b =relative to the bearing
B_i =relative to the i-th mobile reference frame
c =relative to the crank
cr =relative to the connecting rod
p =relative to the piston
I =relative to the inertial reference frame
N =relative to normal reaction forces cylinder-piston
LJB =relative to infinitely long-width journal bearing
SJB =relative to short-width journal bearing
X,Y =relative to the X and Y directions
ξ, η =relative to the radial and transversal directions

Mathematical Modelling

In this section the formulation of representative motion equations to describe the mathematical model of a hermetic reciprocating compressor is developed. The main components of the reciprocating mechanism (i.e., connecting rod and crank) are modelled as rigid bodies, the piston motion is modelled as a particle and the main shaft is modelled as a flexible body via finite elements. Three different approaches which differ in the definition of the restrictive conditions of motion of the centre of the crank have been comparatively studied. These three cases are:

- **Case (I).** Neglecting lateral displacements and tilting oscillations of the crank (no hydrodynamic bearings).
- **Case (II).** Considering lateral displacements but not tilting oscillations of the crank (rigid crankshaft).
- **Case (III).** Considering lateral displacements and tilting oscillations of the crank (flexible crankshaft).

Although the two first approaches make the problem simpler and reduce the computational time, by including the tilting crank effect in the model (case III), a more precise estimation of the journal bearing forces and the journal orbits may be obtained, considering that the oil film thickness is usually only a few micrometers thick. In order to include the tilting oscillations of the crank, the crankshaft is modelled via finite elements and coupled to the motion equations of the piston-slider-crank mechanism through the degrees of freedom where the shaft is connected to the crank. Furthermore, the fluid film forces in the upper and lower bearings are calculated by using analytical solutions of the Reynolds equation, and introduced into the equations of the rotor at each time. Therefore, depending on the case of study, the dynamics of the compressor is described by a different global system of equations.

Developing of the Multibody Dynamics Model

The motion equations of the piston-connecting rod-crank system have been formulated using the Newton-Euler's method, following the methodology suggested by Santos (2001). Figure 2 shows a sketch indicating the inertial referential frame I_{XYZ} and the main angles of rotation for the four moving reference frames.

(a) Definition of the Inertial and Moving Reference Systems.

One inertial reference frame I_{XYZ} and four moving reference frames have been defined. The inertial reference frame is attached to the centre of the bearing (point **O**), whereas, the moving reference frames B_1, B_2 and B_3 are attached to the crank, and the moving reference frame B_4 is attached to the connecting rod. B_1 ($X_1Y_1Z_1$) is obtained by rotating I, the angle β, around the X axis; B_2 ($X_2Y_2Z_2$) is obtained by rotating B_1, the angle Γ, around the Y_1 axis; B_3 ($X_3Y_3Z_3$) is obtained by rotating B_2, the angle θ, around the Z_2 axis, and B_4 ($X_4Y_4Z_4$) is obtained by rotating I, the angle α, around the Z axis. The transformation matrices are given by:

$\mathbf{T}_\beta$: transformation from the inertial frame I to the moving frame B_1.

$$\mathbf{T}_\beta = \begin{bmatrix} 1 & 0 & 0 \\ 0 & \cos\beta & \sin\beta \\ 0 & -\sin\beta & \cos\beta \end{bmatrix}$$

$\mathbf{T}_\Gamma$: transformation from the inertial frame B_1 to the moving frame B_2.

$$\mathbf{T}_\Gamma = \begin{bmatrix} \cos\Gamma & 0 & -\sin\Gamma \\ 0 & 1 & 0 \\ \sin\Gamma & 0 & \cos\Gamma \end{bmatrix}$$

$\mathbf{T}_\theta$: transformation from the inertial frame B_2 to the moving frame B_3.

$$\mathbf{T}_\theta = \begin{bmatrix} \cos\theta & \sin\theta & 0 \\ -\sin\theta & \cos\theta & 0 \\ 0 & 0 & 1 \end{bmatrix}$$

$\mathbf{T}_\alpha$: transformation from the inertial frame I to the moving frame B_4.

$$\mathbf{T}_\alpha = \begin{bmatrix} \cos\alpha & -\sin\alpha & 0 \\ \sin\alpha & \cos\alpha & 0 \\ 0 & 0 & 1 \end{bmatrix}$$

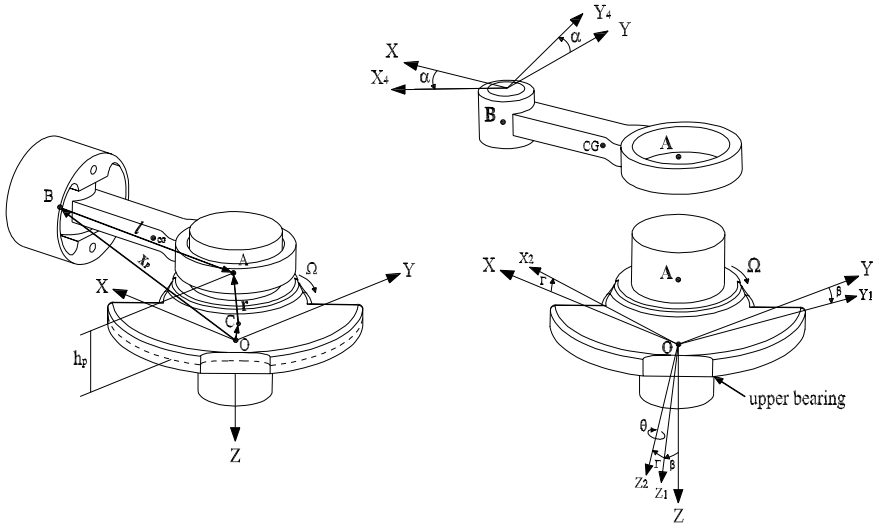

Figure 2. Geometry and reference systems.

(b) Position Vectors and Constraint Equations.

A different constraint equation is established for each one of the three cases studied. A simplified sketch illustrating how the main parts of the system are connected is shown in Fig. 2. The constraint equations for each case are given by Eq. (1-3).

Case (I):

$$ {}_I\mathbf{x}_p + {}_I\mathbf{l} = {}_I\mathbf{r} \tag{1}$$

where,

$$ {}_I\mathbf{r} = \mathbf{T}_\theta^T \cdot {}_{B_3}\mathbf{r} \;;\; {}_{B_3}\mathbf{r} = \{\, r_c \quad 0 \quad -h_p \,\}^{\mathrm{T}} \;;$$
$$ {}_I\mathbf{l} = \{\, -l\cos\alpha \quad l\sin\alpha \quad 0 \,\}^{\mathrm{T}} \;;\; {}_I\mathbf{x}_p = \{\, x_B \quad 0 \quad -h_p \,\}^{\mathrm{T}}$$

Case (II):

$$ {}_I\mathbf{x}_p + {}_I\mathbf{l} = {}_I\mathbf{r} + {}_I\mathbf{c} \tag{2}$$

where, the position vector of the centre of the crank is given by:

$$ {}_I\mathbf{c} = \{\, x_c \quad y_c \quad 0 \,\}^T$$

Case (III):

$$ {}_I\mathbf{x}_p + {}_I\mathbf{l} = {}_I\mathbf{r} + {}_I\mathbf{c} \tag{3}$$

In this case rotations in β and Γ are considered, therefore the vector ${}_I\mathbf{r}$ is given by:

$$ {}_I\mathbf{r} = \mathbf{T}_\beta^T \cdot \mathbf{T}_\Gamma^T \cdot \mathbf{T}_\theta^T \cdot {}_{B_3}\mathbf{r}$$

(c) Kinematic Relations.

The angular velocities for each one of the moving reference frames may be written as in Eq. (4).

$$ {}_I\dot{\boldsymbol{\beta}} = \{\, \dot\beta \quad 0 \quad 0 \,\}^{\mathrm{T}} \;;\; {}_{B_1}\dot{\boldsymbol{\Gamma}} = \{\, 0 \quad \dot\Gamma \quad 0 \,\}^{\mathrm{T}} \;;$$
$$ {}_{B_2}\dot{\boldsymbol{\theta}} = \{\, 0 \quad 0 \quad \dot\theta \,\}^{\mathrm{T}} \;;\; {}_I\dot{\boldsymbol{\alpha}} = \{\, 0 \quad 0 \quad -\dot\alpha \,\}^{\mathrm{T}} \tag{4}$$

For the cases (I) and (II), the absolute angular velocity of the crank is given by $\omega = \dot\theta$, since $\dot\beta$ and $\dot\Gamma$ are equal to zero. Thus, in these cases the moving reference frame B_3 will be simply obtained by rotating *I*, the angle θ, around the Z axis. For the case (III) the absolute angular velocity written with help of the moving reference frame B_3, is given by:

$$ {}_{B_3}\boldsymbol{\omega} = {}_{B_3}\dot{\boldsymbol{\beta}} + {}_{B_3}\dot{\boldsymbol{\Gamma}} + {}_{B_3}\dot{\boldsymbol{\theta}} \tag{5}$$

where:

$$ {}_{B_3}\dot{\boldsymbol{\beta}} = \mathbf{T}_\theta \cdot \mathbf{T}_\Gamma \cdot \mathbf{T}_\beta \cdot {}_I\dot{\boldsymbol{\beta}} \;;$$
$$ {}_{B_3}\dot{\boldsymbol{\Gamma}} = \mathbf{T}_\theta \cdot \mathbf{T}_\Gamma \cdot {}_{B_1}\dot{\boldsymbol{\Gamma}} \;;\; {}_{B_3}\dot{\boldsymbol{\theta}} = \mathbf{T}_\theta \cdot {}_{B_2}\dot{\boldsymbol{\theta}}$$

The expressions to calculate the velocities and accelerations of the piston ($\dot x_B$, $\ddot x_B$) and the connecting rod ($\dot\alpha$, $\ddot\alpha$) are obtained by differentiating the constraint equation for each case respectively, Eq. (6-11).

Case (I):

- Velocities:

$$ \begin{bmatrix} 1 & l\sin\alpha \\ 0 & l\cos\alpha \end{bmatrix} \begin{Bmatrix} \dot x_B \\ \dot\alpha \end{Bmatrix} = \begin{Bmatrix} -r_c\dot\theta\sin\theta \\ r_c\dot\theta\cos\theta \end{Bmatrix} \tag{6}$$

- Accelerations:

$$ \begin{bmatrix} 1 & l\sin\alpha \\ 0 & l\cos\alpha \end{bmatrix} \begin{Bmatrix} \ddot x_B \\ \ddot\alpha \end{Bmatrix} = \begin{Bmatrix} -r_c(\ddot\theta\sin\theta - \dot\theta^2\cos\theta) - l\dot\alpha^2\cos\alpha \\ r_c(\ddot\theta\cos\theta - \dot\theta^2\sin\theta) + l\dot\alpha^2\sin\alpha \end{Bmatrix} \tag{7}$$

Case (II):

- Velocities:

$$\begin{bmatrix} 1 & l\sin\alpha \\ 0 & l\cos\alpha \end{bmatrix}\begin{Bmatrix} \dot{x}_B \\ \dot{\alpha} \end{Bmatrix} = \begin{Bmatrix} -r_c\dot{\theta}\sin\theta + \dot{x}_C \\ r_c\dot{\theta}\cos\theta + \dot{y}_C \end{Bmatrix} \tag{8}$$

- Accelerations:

$$\begin{bmatrix} 1 & l\sin\alpha \\ 0 & l\cos\alpha \end{bmatrix}\begin{Bmatrix} \ddot{x}_B \\ \ddot{\alpha} \end{Bmatrix} = \begin{Bmatrix} -r_c(\ddot{\theta}\sin\theta - \dot{\theta}^2\cos\theta) - l\dot{\alpha}^2\cos\alpha + \ddot{x}_C \\ r_c(\ddot{\theta}\cos\theta - \dot{\theta}^2\sin\theta) + l\dot{\alpha}^2\sin\alpha + \ddot{y}_C \end{Bmatrix} \tag{9}$$

Case (III):

- Velocities

$$\begin{bmatrix} 1 & l\sin\alpha \\ 0 & l\cos\alpha \end{bmatrix}\begin{Bmatrix} \dot{x}_B \\ \dot{\alpha} \end{Bmatrix} = \begin{Bmatrix} w_1 \\ w_2 \end{Bmatrix} \tag{10}$$

- Accelerations:

$$\begin{bmatrix} 1 & l\sin\alpha \\ 0 & l\cos\alpha \end{bmatrix}\begin{Bmatrix} \ddot{x}_B \\ \ddot{\alpha} \end{Bmatrix} = \begin{Bmatrix} w_3 \\ w_4 \end{Bmatrix} \tag{11}$$

where:

$$w_1 = -r_c(\dot{\Gamma}s\Gamma c\theta + \dot{\theta}c\Gamma s\theta) - h_p\dot{\Gamma}c\Gamma + \dot{x}_C \tag{12}$$

$$w_2 = r_c\dot{\beta}(c\beta s\Gamma c\theta - s\beta s\theta) + r_c\dot{\theta}(c\beta c\theta - s\beta s\Gamma s\theta) + \dot{\Gamma}(r_c s\beta c\Gamma c\theta - h_p s\beta s\Gamma) + \dot{\beta}h_p c\beta c\Gamma + \dot{y}_C \tag{13}$$

$$w_3 = -r_c\ddot{\Gamma}s\Gamma c\theta + \dot{\Gamma}^2(h_p s\Gamma - r_c c\Gamma c\theta) + 2r_c\dot{\theta}\dot{\Gamma}s\Gamma s\theta - r_c\dot{\theta}_2 c\Gamma c\theta - h_p\ddot{\Gamma}c\Gamma - r_c\ddot{\theta}c\Gamma s\theta - l\dot{\alpha}^2 c\alpha + \ddot{x}_C \tag{14}$$

$$w_4 = -r_c\dot{\theta}^2(c\beta s\theta + s\beta s\Gamma c\theta) - \dot{\beta}^2(r_c c\beta s\theta + r_c s\beta s\Gamma c\theta + h_p s\beta c\Gamma) - \dot{\Gamma}^2(r_c s\beta s\Gamma c\theta + h_p s\beta c\Gamma) + \ddot{\beta}(h_p c\beta c\Gamma - r_c s\beta s\theta + r_c c\beta s\Gamma c\theta) + \ddot{\Gamma}(r_c s\beta c\Gamma c\theta - h_p s\beta s\Gamma) - 2r_c\dot{\theta}\dot{\beta}(s\beta c\theta + c\beta s\Gamma s\theta) + 2\dot{\beta}\dot{\Gamma}(r_c c\beta c\Gamma c\theta - h_p c\beta s\Gamma) - 2r_c\dot{\theta}\dot{\Gamma}s\Gamma s\beta c\Gamma s\theta + r_c\ddot{\theta}(c\beta c\theta - s\beta s\Gamma s\theta) + l\dot{\alpha}^2 s\alpha + \ddot{y}_C \tag{15}$$

In Eq.(12-15):

$$s\theta = \sin\theta;\quad c\theta = \cos\theta;\quad s\alpha = \sin\alpha;\quad c\alpha = \cos\alpha;$$
$$s\beta = \sin\beta;\quad c\beta = \cos\beta;\quad s\Gamma = \sin\Gamma;\quad c\Gamma = \cos\Gamma.$$

(d) Equations of Motion.

The equations of motion for each body and for the case (III) are given by Eq. (16-20). Since the piston is not the focus of the present analysis, it should be noticed that in the modelling of the piston the friction forces are not included.

Crank

$$\sum {}_I\mathbf{f} = m_c\cdot {}_I\bar{\mathbf{a}}_c \;\Rightarrow\; {}_I\mathbf{f}_A = m_c\{\ddot{x}_c\ ,\ddot{y}_c\}^{\mathrm{T}} \tag{16}$$

$$\sum {}_{B_3}\mathbf{M}_C = {}_{B_3}\mathbf{r}\times{}_{B_3}\mathbf{f}_A + {}_{B_3}\boldsymbol{\tau} = {}_{B_3}\mathbf{I}_c\cdot\frac{d}{dt}\left({}_{B_3}\boldsymbol{\omega}\right) + {}_{B_3}\boldsymbol{\omega}\times\left({}_{B_3}\mathbf{I}_c\cdot{}_{B_3}\boldsymbol{\omega}\right) + m_c\cdot {}_{B_3}\bar{\mathbf{r}}_{C-cm}\times {}_{B_3}\mathbf{a}_C \tag{17}$$

where,

$${}_{B_3}\mathbf{f}_A = \mathbf{T}_\theta\cdot\mathbf{T}_\Gamma\cdot\mathbf{T}_\beta\cdot{}_I\mathbf{f}_A;\quad {}_{B_3}\boldsymbol{\tau} = \{0\ ,0\ ,\tau_z\ \}^{\mathrm{T}};\quad {}_{B_3}\bar{\mathbf{r}}_{C-cm} = \{e_c\ ,0\ ,0\ \}^{\mathrm{T}}$$

Connecting Rod

$$\sum {}_I\mathbf{f} = m_{cr}\cdot {}_I\bar{\mathbf{a}}_{cr} = {}_I\mathbf{f}_A + {}_I\mathbf{f}_B \tag{18}$$

$$\sum {}_{B_4}\mathbf{M}_B = {}_{B_4}\mathbf{l}\times{}_{B_4}\mathbf{f}_A = {}_{B_4}\mathbf{I}_{cr}\cdot\frac{d}{dt}\left({}_{B_4}\boldsymbol{\alpha}\right) + {}_{B_4}\boldsymbol{\alpha}\times\left({}_{B_4}\mathbf{I}_{cr}\cdot{}_{B_4}\boldsymbol{\alpha}\right) + m_{cr}\cdot {}_{B_4}\bar{\mathbf{r}}_{cr}\times {}_{B_4}\mathbf{a}_B \tag{19}$$

where,

$${}_I\bar{\mathbf{a}}_{cr} = {}_I\mathbf{a}_B + {}_I\dot{\boldsymbol{\alpha}}\times{}_I\boldsymbol{\alpha}\times{}_I\bar{\mathbf{r}}_{cr} + {}_I\ddot{\boldsymbol{\alpha}}\times{}_I\bar{\mathbf{r}}_{cr} = \begin{Bmatrix} \ddot{x}_B + \bar{r}_{cr}\left(\dot{\alpha}^2\cos\alpha + \ddot{\alpha}\sin\alpha\right) \\ \bar{r}_{cr}\left(\ddot{\alpha}\cos\alpha - \dot{\alpha}^2\sin\alpha\right) \\ 0 \end{Bmatrix};$$

$${}_{B_4}\mathbf{f}_A = \mathbf{T}_\alpha\cdot{}_I\mathbf{f}_A;\quad {}_{B_4}\mathbf{a}_B = \mathbf{T}_\alpha\cdot{}_I\mathbf{a}_B;\quad {}_I\mathbf{a}_B = \{\ddot{x}_B\ ,0\ ,0\ \}^{\mathrm{T}}$$

Piston

$$\sum {}_I\mathbf{f}_B = m_p\cdot {}_I\mathbf{a}_B = {}_I\mathbf{f}_B + {}_I\mathbf{f}_N + {}_I\mathbf{f}_p \tag{20}$$

where,

$${}_I\mathbf{f}_p = \{P_g\cdot A_p\ ,0\ ,0\ \}^{\mathrm{T}}$$

For each case the equations of motion may be written in a matrix form as in Eq. (21), where the vector $\bar{\mathbf{b}}$ contains the main unknowns (i.e., reaction forces, reaction moments and accelerations). This matrix system is fully described for each case in the appendices A, B and C respectively. For the case (III), where the flexibility of the shaft is included, the matrix system of Eq. (21) has to be coupled to the motion equations of the rotor obtained via a finite elements formulation, which is presented in the next sections.

$$\bar{\mathbf{A}}\cdot\bar{\mathbf{b}} = \bar{\mathbf{c}} \tag{21}$$

Modelling of the Rotor

For the case (III), the main shaft of the compressor is considered as a simply rotating beam, supported by the upper and lower bearings, as illustrated in Fig. 1. The shaft is modelled as a flexible body using a finite elements formulation for a rotor bearing system, which includes gyroscopic and rotatory inertia effects (Nelson and McVaugh, 1976). Considering that the main focus of this study is on the lower mode shapes, the use of this formulation is appropriated to this case and only few finite elements have been used to model the rotor. The global equation of motion can be written as in Eq. (22), where, $\bar{\mathbf{M}}$, $\bar{\mathbf{K}}$, $\bar{\mathbf{G}}$ are the mass, stiffness and gyroscopic matrices respectively, and $\bar{\mathbf{f}}$ is the vector of loads on the rotor, which includes: static preload forces ($ {}_I\mathbf{f}_{pl}$), unbalance rotor forces ($ {}_I\mathbf{f}_{ub}$) and the hydrodynamic bearing forces ($ {}_I\mathbf{f}_b$). Based on the fluid film theory, the bearing forces are calculated by using analytical solutions of the Reynolds equation. These forces depend on the linear displacements and velocities of the nodes that in the finite element model represent the journal bearings centre.

$$\overline{\mathbf{M}}\cdot\ddot{\mathbf{q}} = \underbrace{\overline{\mathbf{f}} - \overline{\mathbf{G}}\cdot\dot{\mathbf{q}} - \overline{\mathbf{K}}\cdot\mathbf{q}}_{\hat{\mathbf{f}}} \tag{22}$$

Fluid Film Forces

The governing equation for the pressure distribution of the oil film in dynamically loaded journal bearings is given by Eq. (23). This equation is obtained from the general formulation of the Reynolds equation (Hamrock, 1991). In this equation, $\dot{\phi}$ is the rotational speed of the journal centre about the bearing centre and ε is the relative eccentricity.

$$\frac{\partial}{\partial\varphi}\left(\frac{h_b^3}{\mu}\frac{\partial p}{\partial\varphi}\right) + r_b^2\frac{\partial}{\partial z}\left(\frac{h_b^3}{\mu}\frac{\partial p}{\partial z}\right) = 12c_b r_b^2\left[\frac{\partial\varepsilon}{\partial t}\cos\varphi + \varepsilon\sin\varphi\left(\frac{\partial\phi}{\partial t} - \frac{\Omega}{2}\right)\right] \tag{23}$$

The main geometric parameters and reference frames used to describe a journal bearing are shown in Fig. 3. The fluid film thickness around the bearing circumference can be calculated by using the expression: $h_b = c_b(1+\varepsilon\cos\varphi)$, where φ is the angle measured from the location of the maximum film thickness. In dynamically loaded bearings, the eccentricity and attitude angle will vary through the loading cycle. Therefore, the fluid film pressure distribution at any eccentricity ratio may be determined only if the normal squeeze velocity ($\dot{\varepsilon}$) and the rotational velocities ($\dot{\phi}, \Omega$) are known for the same eccentricity ratio. Complete solutions of Eq. (23) may be obtained numerically, and solutions for limited cases may be also obtained analytically.

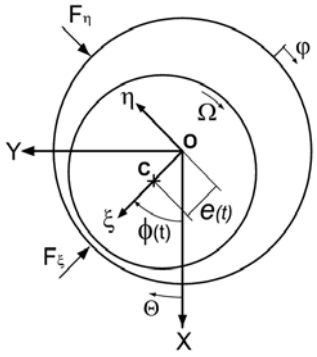

Figure 3. Journal bearing geometry.

In this work, analytical solutions for the short-width bearing (*SJB*) and infinitely-long-width bearing (*LJB*) theories have been used. The short-journal-bearing theory assumes that the variation of pressure is more significant in the axial direction than in the circumferential direction, and therefore the first term on the left side of Eq. (23) can be neglected. In contrast, for an infinitely long-width-journal-bearing, the pressure in the axial direction is assumed to be constant, and therefore the side-leakage term, i.e., the second term on the left side of Eq. (23) can be neglected. Thus, the modified Reynolds equation for each case can be integrated twice and analytical expressions for the pressure distribution can be found. Assuming that the bearing is well aligned and the viscosity of the lubricant keeps constant, the pressure distribution for a *SJB* and a *LJB* is given by Eq. (24-25).

$$p_{SJB} = -\frac{3\mu}{h_b^3}\left(\frac{l_b^2}{4} - z^2\right)\left[\left(\Omega - 2\frac{\partial\phi}{\partial t}\right)\frac{\partial h_b}{\partial\varphi} + 2c_b\cos\varphi\frac{\partial\varepsilon}{\partial t}\right] \tag{24}$$

$$p_{LJB} = 6\mu\left(\frac{r_b}{c_b}\right)^2\left\{\left(\Omega - 2\frac{\partial\phi}{\partial t}\right)\frac{\varepsilon\sin\varphi(2+\varepsilon\cos\varphi)}{(2+\varepsilon^2)(1+\varepsilon\cos\varphi)^2} + \frac{1}{\varepsilon}\frac{\partial\varepsilon}{\partial t}\left[\frac{1}{(1+\varepsilon\cos\varphi)^2} - \frac{1}{(1+\varepsilon)^2}\right]\right\} \tag{25}$$

The journal bearing forces are calculated by integrating the pressure distribution. If the pressure is integrated over all the fluid film around the bearing (i.e, $0 \le \varphi \le 2\pi$), the analytical solution is known as a *full Sommerfeld solution*. However, if the analysis is limited to the convergent film (i.e., $0 \le \varphi \le \pi$), the analytical solution is known as a *half Sommerfeld solution*. Because in real bearings pressures lower than the ambient's are rarely found, and using the last approach more realistic predictions may be obtained (Hamrock, 1991). Thus, the analytical expressions to calculate the bearing forces in ξ, η coordinates, using the half Sommerfeld conditions for the *SJB* and *LJB* approaches respectively, are given by Eq. (26-29). A detailed procedure to obtain these expressions is included in the reference (Frêne, 1990).

- ***Hydrodynamic fluid film forces: Short-journal-bearing***

$$F_\xi = \frac{-r_b\mu l_b^3}{2c_b^2(1-\varepsilon^2)^2}\left[\frac{\pi(1+2\varepsilon^2)}{(1-\varepsilon^2)^{1/2}}\frac{\partial\varepsilon}{\partial t} + 2\varepsilon^2\left(\Omega - 2\frac{\partial\phi}{\partial t}\right)\right] \tag{26}$$

$$F_\eta = \frac{r_b\mu l_b^3\varepsilon}{2c_b^2(1-\varepsilon^2)^2}\left[4\frac{\partial\varepsilon}{\partial t} + \frac{\pi(1-\varepsilon^2)^{1/2}}{2}\left(\Omega - 2\frac{\partial\phi}{\partial t}\right)\right] \tag{27}$$

- ***Hydrodynamic fluid film forces: Infinitely-long-journal-bearing***

$$F_\xi = \frac{-12r_b^3\mu l_b}{c_b^2}\left[\frac{\varepsilon^2}{(2+\varepsilon^2)(1-\varepsilon^2)}\left(\Omega - 2\frac{\partial\phi}{\partial t}\right) + \left(\frac{1}{(1-\varepsilon^2)^{3/2}}\right)\left(\frac{\pi}{2} - \frac{8}{\pi(2+\varepsilon^2)}\right)\frac{\partial\varepsilon}{\partial t}\right] \tag{28}$$

$$F_\eta = \frac{12r_b^3\mu l_b}{c_b^2}\left[\frac{\pi\varepsilon}{2(2+\varepsilon^2)(1-\varepsilon^2)^{1/2}}\left(\Omega - 2\frac{\partial\phi}{\partial t}\right) + \left(\frac{2\varepsilon}{(2+\varepsilon^2)(1-\varepsilon^2)}\right)\frac{\partial\varepsilon}{\partial t}\right] \tag{29}$$

In order to describe the fluid film forces in the inertial reference frame, the transformation given by Eq. (30) is used, where the attitude angle $\phi(t)$ is the angle measured between the X-axis and the location of the minimum oil film thickness. For the case (II), the bearing forces F_X and F_Y are coupled directly to the vector $\overline{\mathbf{c}}$ of Eq. (21), whereas, for the case (III), they correspond to the components of the vector ${}_I\mathbf{f}_b$ of Eq. (22).

$$\begin{Bmatrix} F_X \\ F_Y \end{Bmatrix} = \begin{bmatrix} \cos\phi(t) & -\sin\phi(t) \\ \sin\phi(t) & \cos\phi(t) \end{bmatrix}\begin{Bmatrix} F_\xi \\ F_\eta \end{Bmatrix} \tag{30}$$

Numerical Implementation

The equations of motion that describe the dynamics of the system together with the *FEM* model of the shaft and the analytical expressions for the fluid film forces yield to a system of high complexity and non-linearity. A flowchart, with the main steps

involved in the numerical algorithm implemented to solve the system of equations, is shown in Fig. 4. In this case, a Newmark implicit method combined with a predictor-corrector approach has been used (Garcia, 1994). The simulation procedure is summarized in the following four main steps:

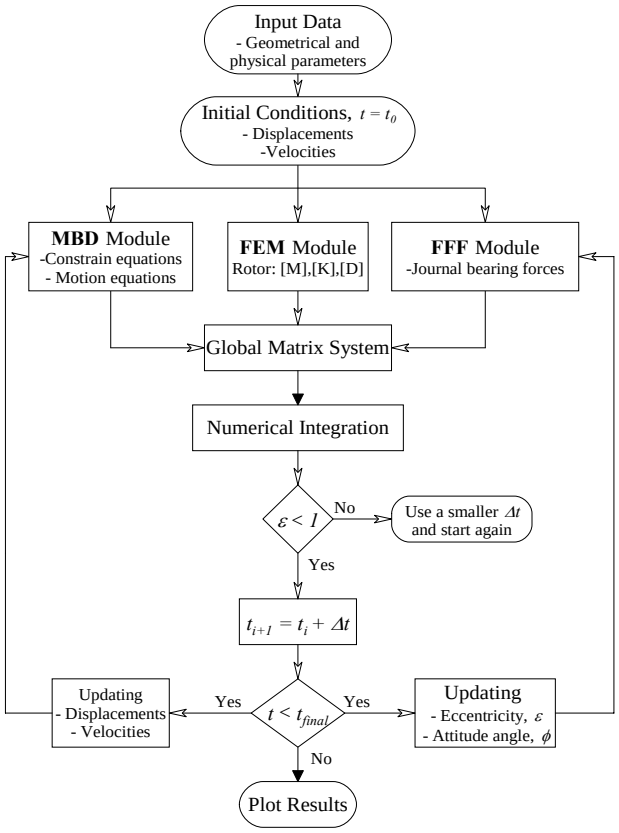

Figure 4. Flow chart of the computer code.

a) *Input data and starting values*. In this part, the geometrical and physical parameters must be given, i.e., dimensions, rotational speed, mass, inertia, preloads, etc. Starting values, such as initial displacements and velocities of the journal bearings centre, should be also given.

b) *Pre-processing*. This part includes the generation of structural matrices of the multibody model (MBD module) and the matrices of the flexible rotor (FEM module). Initial fluid film forces can be computed within the FFF module, based on the given initial conditions.

c) *Numerical computation*. This is the main core of the code, which includes the coupling of matrices, the computation of the journal bearing forces at each time step and the numerical solution of the global system. For the cases (I) and (II), the global systems of equations to be numerically solved are included in appendixes A and B respectively. However, for the case (III), the system of equations shown in appendix C must be coupled to the equations of the rotor. In order to couple the MBD matrix system given by Eq. (21) to the equations of the flexible rotor given by Eq. (22), the matrix $\overline{\mathbf{M}}$ (size $ndof \times ndof$) is coupled to the matrix $\overline{\mathbf{A}}$ (size 16×16) in the degrees of freedom related to the linear and angular accelerations of the crank centre ($\ddot{q}_1, \ddot{q}_2, \ddot{q}_3, \ddot{q}_4$), obtaining the global mass matrix $\tilde{\mathbf{M}}$ (size $ndof + 12$). Similarly, the vector $\hat{\mathbf{f}}$, which is the resultant right hand side vector of Eq. (22), is coupled to the vector $\overline{\mathbf{c}}$ of Eq. (21). Thus, the global matrix system for case (III) can be written as in Eq. (31).

$$\tilde{\mathbf{M}} \cdot \tilde{\mathbf{b}} = \tilde{\mathbf{c}} \tag{31}$$

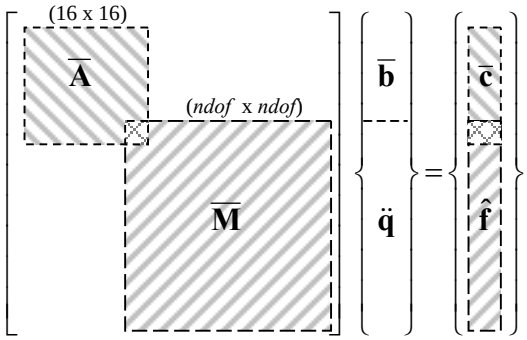

where,

$$\overline{\mathbf{b}} = \left\{ f_{B_x}, f_{B_y}, f_{B_z}, N_y, N_z, f_{A_x}, f_{A_y}, f_{A_z}, f_{C_z}, \ddot{\theta}, \ddot{x}_B, \ddot{\alpha} \right\}^{\mathrm{T}} ;$$

$$\ddot{\mathbf{q}} = \left\{ \ddot{q}_1, \ddot{q}_2, \ldots, \ddot{q}_{ndof} \right\}^{\mathrm{T}}$$

When the system of Eq. (31) is initially solved, the initial forces and accelerations ($\tilde{\mathbf{b}}_0$) are calculated from the initial conditions, computing: $\tilde{\mathbf{M}}_{t_0}^{-1} \cdot \tilde{\mathbf{c}}_{t_0}$. Using the Newmark implicit method, the iterative equations are given by Eq. (32-34).

$$\left\{ \overline{\mathbf{b}}_{t_{i+1}}, \ddot{\mathbf{q}}_{t_{i+1}} \right\}^{\mathrm{T}} = \tilde{\mathbf{M}}_{t_{i+1}}^{-1} \cdot \tilde{\mathbf{c}}_{t_{i+1}} \tag{32}$$

$$\dot{q}_{t_{i+1}} = \dot{q}_{t_i} + \Delta t \left[\left(1 - \hat{\gamma}\right) \ddot{q}_{t_i} + \hat{\gamma}\, \ddot{q}_{t_{i+1}} \right] \tag{33}$$

$$q_{t_{i+1}} = q_{t_i} + \Delta t\, \dot{q}_{t_i} + \frac{\Delta t^2}{2} \left[\left(1 - 2\hat{\beta}\right) \ddot{q}_{t_i} + 2\hat{\beta}\, \ddot{q}_{t_{i+1}} \right] \tag{34}$$

To compute $\ddot{q}_{t_{i+1}}$, the elements of the vector $\tilde{\mathbf{c}}_{t_{i+1}}$ must be estimated in advance, which implies to calculate first the journal bearing forces $\mathbf{f}_b$ at the time t_{i+1}. Since the bearing forces depend on the instantaneous position and velocities of the journal centre, the Heun's explicit method is used to predict initial guesses for $\dot{q}_{t_{i+1}}^0$ and $q_{t_{i+1}}^0$. Then, using Eq. (32-34) $\ddot{q}_{t_{i+1}}^1$ can be calculated, as well as new estimated values for $\dot{q}_{t_{i+1}}^1$ and $q_{t_{i+1}}^1$ respectively. These new estimated values are used to update the journal bearing forces and then, using again Eq. (32) a new estimate for $\ddot{q}_{t_{i+1}}^2$ can be obtained, and so on until the difference of two consecutive values becomes smaller than the prescribed tolerance given. Additionally, the explicit Euler method of first order is used to estimate the crank angle θ_{t_i} and the instantaneous angular velocity.

d) *Post-processing*. This part includes the generation of plots of journal bearing orbits, journal bearing forces, maximum oil film pressure, minimum fluid film thickness, reaction forces and reaction moments as a function of the time and the rotational crank angle during each cycle.

Results and Discussion

The system of equations described in the previous sections has been numerically solved for each one of the three approaches presented. Particularly, the numerical results have been analysed with focus on the behaviour of the main bearing of the crankshaft (upper journal bearing shown in Fig. 1. The main geometrical dimensions and physical properties of the reciprocating compressor used in this study are given in table 1. The gas pressure as a function of the crank angle is taken from Cho and Moon (2005) and it is shown in Fig. 5a. The variation of torque in function of the angular velocity for a hermetic compressor with similar characteristics to the one used in this work is taken from Rigola (2002) and it is shown in Fig. 5b.

Table 1. Main geometrical and physical parameters.

Radius crank-pin centre	r_c	7.5 *mm*
Radius of bearings	r_b	8 *mm*
Width of bearings	l_b	6 *mm*
Journal clearance	c_b	15 μm
Length crank pin	h_p	10 *mm*
Distance between bearings	L	80 *mm*
Inertia of motor-rotor		I_x, I_y = 0.4x10^{-3} ; I_z = 0.1x10^{-2} *kg.m*^{2}
Diameter of piston	D_p	23 *mm* (A_p = 415.5 *mm*^{2})
Length of the piston	l_p	22 *mm*
Mass of the piston	m_p	0.043 *kg*
Lubricant viscosity	μ	0.005 *Pa.s*
Angular velocity	Ω	312 *rad/s* (2980 *rpm)*
Mass eccentricity of crank	e_c	5 *mm*

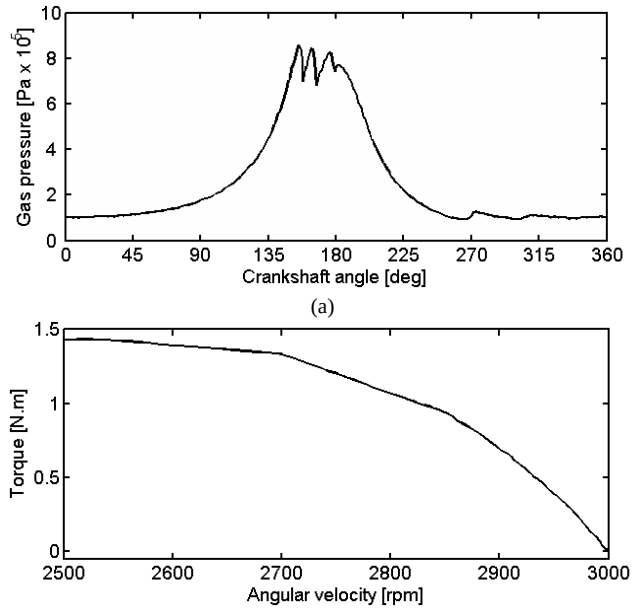

Figure 5. (a) Curve of the gas pressure (Pg) as a function of the crankshaft angle. (b) Curve of the motor torque (τ_z) as a function of the angular velocity.

Results - Case (I)

In this case, lateral displacements and tilting oscillations of the crank are neglected. Therefore, the hydrodynamic bearing forces are not calculated, but instead the reaction forces and the reaction moments at the centre of the crank are calculated. The reaction forces in the joint crank pin-connecting rod ($\mathbf{f}_A$) and in the joint piston-connecting rod ($\mathbf{f}_B$) are shown in Fig. 6. The plot of the reaction moments is shown in Fig. 7. The maximum forces are found close to the top dead centre and it can be seen clearly that the reaction forces in *X*-direction are dominated by the compression force coming from the piston and the inertial effects.

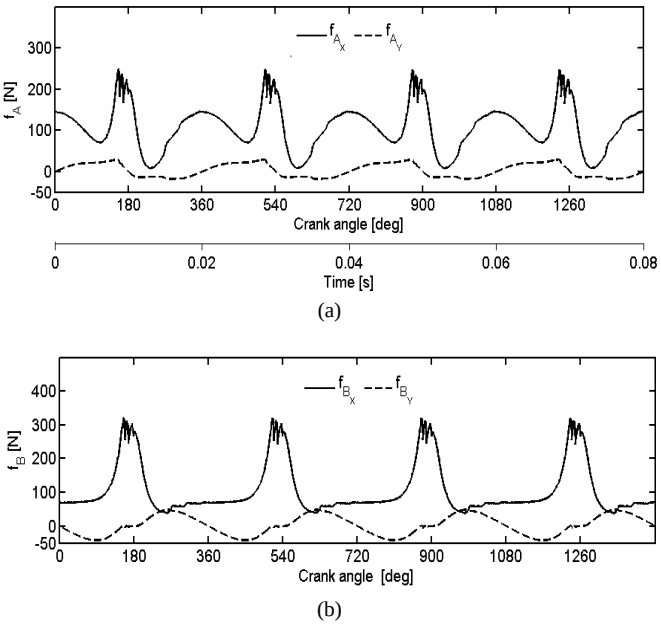

Figure 6. Reaction forces. (a) Joint piston-connecting rod. (b) Joint crank-connecting rod – case(I).

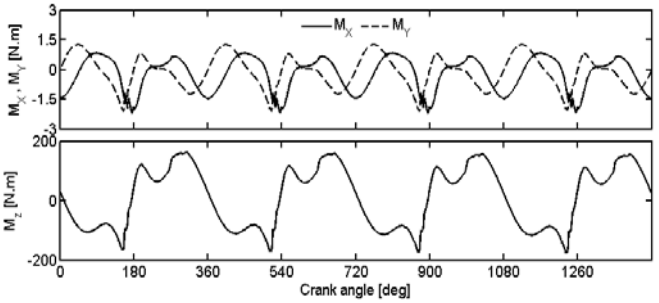

Figure 7. Crank reaction moments – case (I).

Results - Case (II)

In this case, tilting oscillations of the crank are neglected and lateral displacements are allowed. The hydrodynamic journal forces for the upper bearing are computed using Eq. (26-27) and they are shown in Fig. 8. It can be seen from this figure that the upper bearing forces are similar to the reaction forces obtained for case (I), which is expected, due to the fact that the equilibrium conditions have to be always accomplished, even if the crank centre is allowed to have lateral oscillations.

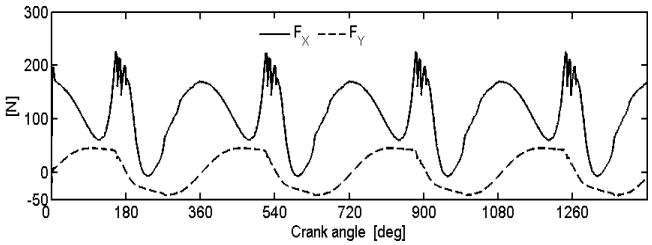

Figure 8. Journal bearing forces – case (II).

The orbit of the journal centre for the upper bearing using the *SJB* approach is shown in Fig. 9. The orbit obtained has a similar shape compared to predicted orbits of main bearings of internal combustion engines (Ritchie, 1975; Pal, 1988). The maximum fluid film pressure is computed for each crank angle during four cycles, as shown in Fig. 10. It can be observed that the highest values of hydrodynamic pressure in the bearings are found at each cycle around the top dead centre position of the piston, i.e., when the pressure in the cylinder is maximum.

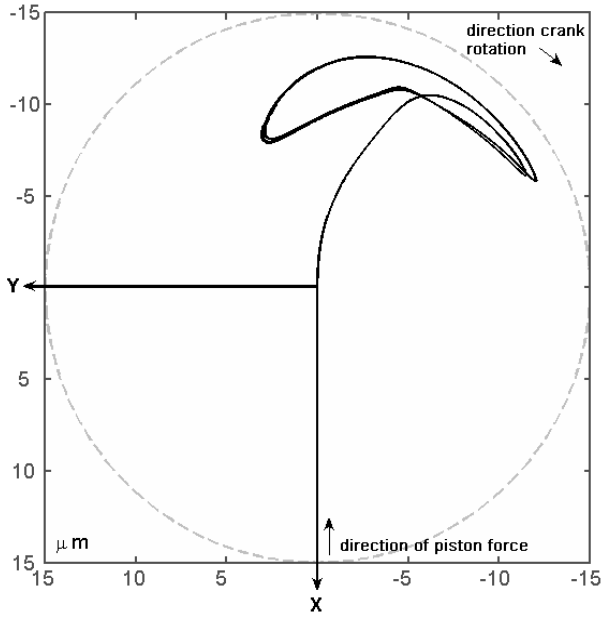

Figure 9. Orbit journal centre – case (II).

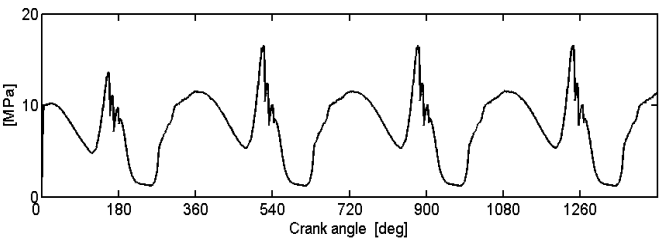

Figure 10. Maximum fluid film pressure – case (II).

Results - Case (III)

In this case, lateral displacements and tilting oscillations of the crank are allowed. Therefore, the matrix system of equations of the multibody model is coupled to the equations of the finite elements formulation of the crankshaft. Considering that this study is more focused on the hydrodynamic behaviour of the journal bearings than in the dynamics of the crankshaft, only four finite elements were used for the calculations, which are enough to include the flexible supports (journal bearings), crank and rotor unbalance, and to describe the tilting oscillations of the crank. Moreover, the main interest is to cover frequency range from 0 to 5000 Hz. Using a linearized model for the journal bearings the first and second bending eigenfrequencies of the shaft are around 1050 Hz and 6810 Hz respectively. Following the flow chart of Fig. 4, the global system of equations was solved by using a time step of $\Delta t = 1e\text{-}6s$, in order to ensure convergence of the solution.

The fluid film forces computed for the upper and lower bearings are shown in Fig. 11. It can be seen from this figure that the upper bearing forces are similar to the ones obtained for case (II), however, in this case, small transient oscillations occur during the first cycles of the crank rotation. The transient oscillations are more evident in the plot of the lower bearing forces, since the fluid film forces for this bearing are much lower compared to the upper bearing forces. During the numerical simulations, it was noticed that these oscillations are of numerical origin, caused by the initial conditions adopted. The transient response disappears after the first cycles and the system operates under steady-state conditions.

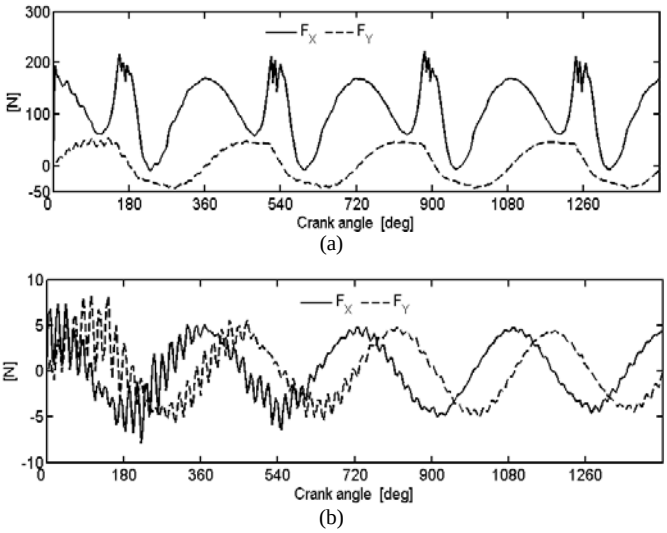

Figure 11. Journal bearing forces. (a) Upper bearing, (b) Lower bearing – case (III).

The minimum fluid film thickness for the upper bearing is plotted in Fig. 12a. It is observed in this figure that the lowest values of oil film thickness are found during the gas compression cycle, at approximately $65deg$ before the piston reaches the top dead centre (i.e., when $\theta \approx 115deg$, $\theta \approx 475deg$, $\theta \approx 835deg$,…). When the plot of minimum fluid film thickness is compared with the plot of maximum pressure, shown in Fig. 12b, it can be seen that the highest pressures values occur at approximately $30deg$ after the lowest fluid film thickness is reached during each cycle.

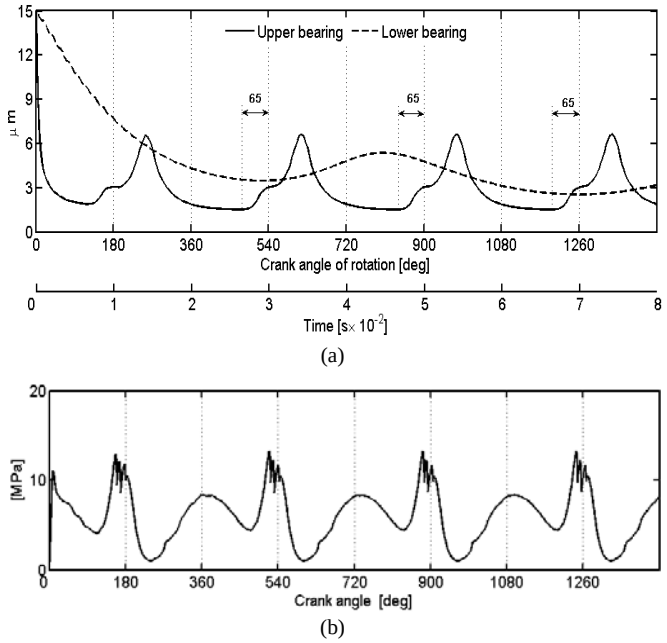

Figure 12. (a) Minimum fluid film thickness. (b) Maximum pressure – upper journal bearing – case(III).

The effect of including the length of the crank pin (h_p) on the behaviour of the upper bearing has been studied through the comparison of orbits and curves of the minimum fluid film thickness, obtained for two different values of h_p. Figure 13a shows the journal orbits obtained for cases (II) and (III) using $h_p = 10mm$ and $h_p = 0$. It is shown in the figure that the influence of the parameter h_p in the orbits is more significant for case (III) than for case (II). This is explained by the fact that in the cases (I) and (II), tilting oscillations of the crank are not allowed, therefore, transversal moments over the crank due to the reaction force $\mathbf{f}_A$ are equilibrated by the reaction moments M_X and M_Y, as shown in Fig. 7. The influence of the parameter h_p on the variation of the minimum fluid film thickness for case (III) can be observed in Fig. 13b. Despite the fact that the difference between the two plots does not seem to be significant, it is found that at some crank positions (e.g., when $\theta = 1180deg$) the difference between the two film thicknesses may be as high as 18%. Therefore, in order to estimate more accurately the effect of the tilting oscillations of the crank on the behaviour of the bearings, it is relevant to include the parameter h_p in the multibody model of the compressor.

The difference between the maximum hydrodynamic pressures computed by using the *SJB* and *LJB* approaches respectively can be significant, as it can be seen in Fig. 14. Thus, in order to ensure a better estimation of the load carrying capacity, and taking into consideration that the bearings of the compressor used for this study are short ($l_b \backslash r_b = 0.75$), all the results presented in this section were obtained by using the *SJB* approach.

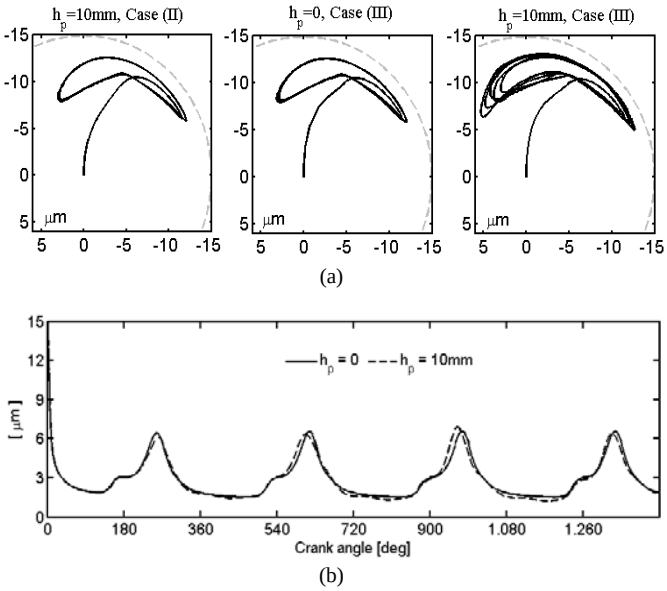

Figure 13. Effect of the crank pin length (hp). (a) Orbits. (b) Minimum fluid film thickness.

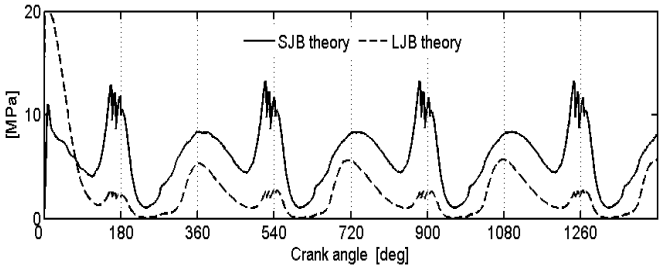

Figure 14. Maximum fluid film pressure using the SJB and LJB approaches.

Conclusions and Further Aspects

Three different approaches for the modelling of a hermetic reciprocating compressor have been analysed in this work. It was found that when the lateral and tilting vibration of the crank are included in the model, more precise estimations of the minimum film thickness are obtained. However, no significant differences were found in the estimation of the hydrodynamic journal bearing forces and the fluid film pressures between the different cases studied. The maximum forces and the minimum film thickness are obtained when the piston is close to the top dead centre. Furthermore, a delay of approximately 30*deg* between the lowest value of the minimum oil film thickness and the maximum fluid film pressure at each cycle was found. The results showed that the nonlinear behaviour of the orbits increases due to the tilting oscillations of the crank, influenced by the length of the crank pin. The increase of the minimum fluid film thickness and the reduction of the bearing vibrations seem to be feasible by modifying the hydrodynamic lubrication conditions through the implementation of a controllable lubrication system based on the periodic behaviour of the bearing performance. In order to develop such a system, further work will be carried out.

Acknowledgments

The authors gratefully acknowledge the support given by the Programme Alβan, the European Union Programme of High Level Scholarships for Latin America, scholarship No. E06D101992CO.

References

Cho, J. R. and Moon, S.J., 2005, "A Numerical Analysis of the Interaction between the Piston Oil Film and the Component Deformation in a Reciprocating Compressor", *Tribology International*, Vol.38, pp. 459-468.

Dufour, R., Der Hagopian, J. and Lalanne, M., 1995, "Transient and Steady State Dynamic Behaviour of Single Cylinder Compressors: Prediction and Experiments", *Journal of Sound and Vibration*, Vol.181, pp. 23-41.

Frêne, J., Nicolas, D., Degueurce, B., Berthe, D. and Godet, M., 1990, "Lubrification Hydrodynamique", Ed. Eyrolles, Paris, 488 p.

Garcia de Jalon, J. and Bayo, E., 1994, "Kinematic and Dynamic Simulation of Multibody Systems", Ed. Springer-Verlag, New-York, 440 p.

Gommed, K. and Etsion, I., 1993, "Dynamic Analysis of Gas Lubricated Reciprocating Ringless Pistons - Basic Modelling", *Journal of Tribology*, Vol.115, pp. 207-213.

Hamrock, B. J., 1991, "Fundamental of Fluid Film Lubrication", NASA Reference Publication, USA, 635 p.

Kim, T. J. and Han, J. S., 2004, "Comparison of the Dynamic Behavior and Lubrication Characteristics of a Reciprocating Compressor Crankshaft in Both Finite and Short Bearing Models", *Tribology Transactions*, Vol.47, No.1, pp. 61-69.

Longo, G. and Gasparella, A. 2003, "Unsteady State Analysis of the Compression Cycle of a Hermetic Reciprocating Compressor", *International Journal of Refrigeration*, Vol.26, pp. 681-689.

Nelson, H. D. and McVaugh, J. M., 1976, "The dynamics of Rotor-Bearing Systems Using Finite Elements", *Journal of Engineering for Industry*, Vol.98, pp. 593-600.

Pal, R., Sinhasan, R. and Singh, D.V, 1988, "Analysis of a Big-End Bearing - a Finite Element Approach", *Wear*, Vol.121, No.1, pp. 117-120.

Rasmussen, B.D., 1997, "Variable Speed Hermetic Reciprocating Compressors for Domestic Refrigerators", Ph.D. Thesis, Technical University of Denmark, Lyngby, Denmark, Vol.1, 158 p.

Rigola, S. J., 2002, "Numerical Simulation and Experimental Validation of Hermetic Reciprocating Compressors", Ph.D. Thesis, Universidad Politécnica de Cataluña, Barcelona, Spain, 109 p.

Ritchie, G.S., 1975, "The Prediction of Journal Loci in Dynamically Loaded Internal Combustion Engine Bearings", *Wear*, Vol.35, No.2, pp. 291-297.

Santos, I. F., 2001, "Dinâmica de Sistemas Mecanicos", Ed. Makron Books, Sao Paulo, Brasil, 272 p.

Appendix A.

Full Matrix of the Multibody Dynamic Model – **Case (I):** $[\overline{\mathbf{A}}]_{\mathbf{I}} \cdot \{\overline{\mathbf{b}}\}_{\mathbf{I}} = \{\overline{\mathbf{c}}\}_{I}$

$$\begin{bmatrix}
1 & 0 & 0 & 0 & 0 & 0 & 0 & 0 & 0 & 0 & 0 & 0 & 0 & m_p & 0 \\
0 & -1 & 0 & 1 & 0 & 0 & 0 & 0 & 0 & 0 & 0 & 0 & 0 & 0 & 0 \\
0 & 0 & 1 & 0 & -1 & 0 & 0 & 0 & 0 & 0 & 0 & 0 & 0 & 0 & 0 \\
1 & 0 & 0 & 0 & 0 & -1 & 0 & 0 & 0 & 0 & 0 & 0 & 0 & -m_{cr} & -m_{cr}\bar{r}_{cr}s\alpha \\
0 & 1 & 0 & 0 & 0 & 0 & -1 & 0 & 0 & 0 & 0 & 0 & 0 & 0 & -m_{cr}\bar{r}_{cr}c\alpha \\
0 & 0 & 1 & 0 & 0 & 0 & 0 & 1 & 0 & 0 & 0 & 0 & 0 & 0 & 0 \\
0 & 0 & 0 & 0 & 0 & 1 & 0 & 0 & -1 & 0 & 0 & 0 & 0 & 0 & 0 \\
0 & 0 & 0 & 0 & 0 & 0 & 1 & 0 & 0 & -1 & 0 & 0 & 0 & 0 & \\
0 & 0 & 0 & 0 & 0 & 0 & 0 & 1 & 0 & 0 & 1 & 0 & 0 & 0 & \\
0 & 0 & 0 & 0 & 0 & 0 & 0 & l & 0 & 0 & 0 & 0 & 0 & 0 & \\
0 & 0 & 0 & 0 & 0 & ls\alpha & lc\alpha & 0 & 0 & 0 & 0 & 0 & 0 & m_{cr}\bar{r}_{cr}s\alpha & I_{cr_Z} \\
0 & 0 & 0 & 0 & 0 & 0 & 0 & 0 & 0 & 0 & 0 & c\theta & s\theta & 0 & 0 \\
0 & 0 & 0 & 0 & 0 & 0 & 0 & r_C & 0 & 0 & 0 & -s\theta & c\theta & 0 & 0 \\
0 & 0 & 0 & 0 & 0 & r_C s\theta & -r_C c\theta & 0 & 0 & 0 & 0 & 0 & 0 & I_{c_Z} & 0 \\
0 & 0 & 0 & 0 & 0 & 0 & 0 & 0 & 0 & 0 & 0 & 0 & 0 & r_C s\theta & 1 \\
0 & 0 & 0 & 0 & 0 & 0 & 0 & 0 & 0 & 0 & 0 & 0 & 0 & -r_C c\theta & 0
\end{bmatrix}
\begin{Bmatrix}
f_{B_X} \\ f_{B_Y} \\ f_{B_Z} \\ N_Y \\ N_Z \\ f_{A_X} \\ f_{A_Y} \\ f_{A_Z} \\ f_{C_X} \\ f_{C_Y} \\ f_{C_Z} \\ M_{C_X} \\ M_{C_Y} \\ \ddot{\theta} \\ \ddot{x}_B \\ \ddot{\alpha}
\end{Bmatrix} =
\begin{Bmatrix}
-P_g A_p \\ 0 \\ -m_p g \\ m_{cr}\dot{\alpha}^2\bar{r}_{cr}c\alpha \\ -m_{cr}\dot{\alpha}^2\bar{r}_{cr}s\alpha \\ m_{cr}g \\ 0 \\ 0 \\ m_c g \\ \bar{r}_{cr}m_{cr}g \\ 0 \\ 0 \\ 0 \\ \tau_z \\ -r_C\dot{\theta}^2 c\theta - l\dot{\alpha}^2 c\alpha \\ -r_C\dot{\theta}^2 s\theta - l\dot{\alpha}^2 s\alpha
\end{Bmatrix}$$

Appendix B

Full Matrix of the Multibody Dynamic Model – **Case (II):** $[\overline{A}]_{II} \cdot \{\overline{b}\}_{II} = \{\overline{c}\}_{II}$

$$\begin{bmatrix}
1 & 0 & 0 & 0 & 0 & 0 & 0 & 0 & 0 & 0 & 0 & 0 & m_p & 0 & 0 & 0 \\
0 & -1 & 0 & 1 & 0 & 0 & 0 & 0 & 0 & 0 & 0 & 0 & 0 & 0 & 0 & 0 \\
0 & 0 & 1 & 0 & -1 & 0 & 0 & 0 & 0 & 0 & 0 & 0 & 0 & 0 & 0 & 0 \\
1 & 0 & 0 & 0 & 0 & -1 & 0 & 0 & 0 & 0 & 0 & -m_{cr} & 0 & 0 & -m_{cr}\bar{r}_{cr}s\alpha & 0 \\
0 & 1 & 0 & 0 & 0 & 0 & -1 & 0 & 0 & 0 & 0 & 0 & 0 & 0 & -m_{cr}\bar{r}_{cr}c\alpha & 0 \\
0 & 0 & 1 & 0 & 0 & 0 & 0 & 1 & 0 & 0 & 0 & 0 & 0 & 0 & 0 & 0 \\
0 & 0 & 0 & 0 & 0 & 0 & 0 & 1 & 1 & 0 & 0 & 0 & 0 & 0 & 0 & 0 \\
0 & 0 & 0 & 0 & 0 & 0 & 0 & l & 0 & 0 & 0 & 0 & 0 & 0 & 0 & 0 \\
0 & 0 & 0 & 0 & 0 & ls\alpha & lc\alpha & 0 & 0 & 0 & 0 & 0 & m_{cr}\bar{r}_{cr}s\alpha & I_{cr_Z} & 0 & 0 \\
0 & 0 & 0 & 0 & 0 & 0 & 0 & 0 & 0 & c\theta & s\theta & 0 & 0 & 0 & 0 & 0 \\
0 & 0 & 0 & 0 & 0 & 0 & 0 & r_C & 0 & -s\theta & c\theta & 0 & 0 & 0 & 0 & 0 \\
0 & 0 & 0 & 0 & 0 & -r_C s\theta & -r_C c\theta & 0 & 0 & 0 & 0 & I_{c_Z} & 0 & 0 & 0 & 0 \\
0 & 0 & 0 & 0 & 0 & 0 & 0 & 0 & 0 & 0 & 0 & -r_c s\alpha & 1 & ls\alpha & -1 & 0 \\
0 & 0 & 0 & 0 & 0 & 0 & 0 & 0 & 0 & 0 & 0 & -r_c c\alpha & 0 & lc\alpha & 0 & -1 \\
0 & 0 & 0 & 0 & 0 & -1 & 0 & 0 & 0 & 0 & 0 & 0 & 0 & 0 & m_C & 0 \\
0 & 0 & 0 & 0 & 0 & 0 & -1 & 0 & 0 & 0 & 0 & 0 & 0 & 0 & 0 & m_C
\end{bmatrix}
\begin{Bmatrix}
f_{B_X} \\ f_{B_Y} \\ f_{B_Z} \\ N_Y \\ N_Z \\ f_{A_X} \\ f_{A_Y} \\ f_{A_Z} \\ f_{C_Z} \\ M_{C_X} \\ M_{C_Y} \\ \ddot{\theta} \\ \ddot{x}_B \\ \ddot{\alpha} \\ \ddot{x}_C \\ \ddot{y}_C
\end{Bmatrix} =
\begin{Bmatrix}
-P_g A_p \\ 0 \\ -m_p g \\ m_{cr}\dot{\alpha}^2\bar{r}_{cr}c\alpha \\ -m_{cr}\dot{\alpha}^2\bar{r}_{cr}s\alpha \\ m_{cr}g \\ m_c g \\ \bar{r}_{cr}m_{cr}g \\ 0 \\ 0 \\ 0 \\ \tau_z \\ -r_C\dot{\theta}^2 c\theta - l\dot{\alpha}^2 c\alpha \\ -r_C\dot{\theta}^2 s\theta - l\dot{\alpha}^2 s\alpha \\ F_X \\ F_Y
\end{Bmatrix}$$

Appendix C

Full Matrix of the Multibody Dynamic Model – **Case (III):** $[\overline{A}]_{III} \cdot \{\overline{b}\}_{III} = \{\overline{c}\}_{III}$

$$\begin{bmatrix}
1 & 0 & 0 & 0 & 0 & 0 & 0 & 0 & 0 & 0 & m_p & 0 & 0 & 0 & 0 & 0 \\
0 & 1 & 0 & -1 & 0 & 0 & 0 & 0 & 0 & 0 & 0 & 0 & 0 & 0 & 0 & 0 \\
0 & 0 & 1 & 0 & -1 & 0 & 0 & 0 & 0 & 0 & 0 & 0 & 0 & 0 & 0 & 0 \\
-1 & 0 & 0 & 0 & 0 & 1 & 0 & 0 & 0 & 0 & m_{cr} & m_{cr}\bar{r}_{cr}s\alpha & 0 & 0 & 0 & 0 \\
0 & -1 & 0 & 0 & 0 & 0 & 1 & 0 & 0 & 0 & 0 & m_{cr}\bar{r}_{cr}c\alpha & 0 & 0 & 0 & 0 \\
0 & 0 & 1 & 0 & 0 & 0 & 0 & 1 & 0 & 0 & 0 & 0 & 0 & 0 & 0 & 0 \\
0 & 0 & 0 & 0 & 0 & 0 & 0 & l & 0 & 0 & 0 & 0 & 0 & 0 & 0 & 0 \\
0 & 0 & 0 & 0 & 0 & ls\alpha & lc\alpha & 0 & 0 & 0 & m_{cr}\bar{r}_{cr}s\alpha & I_{cr_Z} & 0 & 0 & 0 & 0 \\
0 & 0 & 0 & 0 & 0 & 0 & 0 & -1 & 1 & 0 & 0 & 0 & 0 & 0 & 0 & 0 \\
0 & 0 & 0 & 0 & 0 & C_1 & C_2 & C_3 & 0 & -I_{c_Z} - I_{m_Z} & 0 & 0 & -m_c e_c s\Gamma & -m_c e_c s\beta c\Gamma & -I_{c_Z} s\Gamma & 0 \\
0 & 0 & 0 & 0 & 0 & 0 & 0 & 0 & 0 & r_c c\Gamma s\theta & 1 & ls\alpha & -1 & 0 & 0 & C_4 \\
0 & 0 & 0 & 0 & 0 & 0 & 0 & 0 & 0 & C_5 & 0 & lc\alpha & 0 & -1 & C_6 & C_7 \\
0 & 0 & 0 & 0 & 0 & -1 & 0 & 0 & 0 & 0 & 0 & 0 & m_c & 0 & 0 & 0 \\
0 & 0 & 0 & 0 & 0 & 0 & -1 & 0 & 0 & 0 & 0 & 0 & 0 & m_c & 0 & 0 \\
0 & 0 & 0 & 0 & 0 & -h_p C_1 r_c^{-1} & -h_p C_2 r_c^{-1} & -h_p C_3 r_c^{-1} & 0 & 0 & 0 & 0 & 0 & 0 & I_{c_X} c\Gamma c\theta & I_{c_X} s\theta \\
0 & 0 & 0 & 0 & 0 & C_8 & C_9 & C_{10} & 0 & 0 & 0 & 0 & C_{11} & C_{12} & -I_{c_Y} c\Gamma s\theta & I_{c_Y} c\theta
\end{bmatrix}
\begin{Bmatrix}
f_{B_X} \\ f_{B_Y} \\ f_{B_Z} \\ N_Y \\ N_Z \\ f_{A_X} \\ f_{A_Y} \\ f_{A_Z} \\ f_{C_Z} \\ \ddot{\theta} \\ \ddot{x}_B \\ \ddot{\alpha} \\ \ddot{x}_C \\ \ddot{y}_C \\ \ddot{\beta} \\ \ddot{\Gamma}
\end{Bmatrix} =
\begin{Bmatrix}
-P_g A_p \\ 0 \\ -m_p g \\ -m_{cr}\dot{\alpha}^2\bar{r}_{cr}c\alpha \\ -m_{cr}\dot{\alpha}^2\bar{r}_{cr}s\alpha \\ m_{cr}g \\ \bar{r}_{cr}m_{cr}g \\ 0 \\ m_c g \\ \dot{\beta}\dot{\Gamma}I_{c_Z}c\Gamma - \tau_z \\ C_{13} \\ C_{14} \\ 0 \\ 0 \\ C_{15} \\ C_{16}
\end{Bmatrix}$$

where:

$$
\begin{aligned}
C_1 &= -r_c c\Gamma s\theta \\
C_2 &= r_c(c\beta c\theta - s\beta s\Gamma s\theta) \\
C_3 &= r_c(c\beta s\Gamma s\theta - s\beta c\Gamma) \\
C_4 &= r_c s\Gamma c\theta + h_p c\Gamma \\
C_5 &= r_c(s\beta s\Gamma s\theta - c\beta c\theta) \\
C_6 &= r_c(s\beta s\theta - c\beta s\Gamma c\theta) - h_p c\beta c\Gamma \\
C_7 &= -r_c s\beta c\Gamma c\theta + h_p s\beta s\Gamma \\
C_8 &= r_c s\Gamma + h_p c\Gamma c\theta \\
C_9 &= -r_c s\beta c\Gamma + h_p(s\beta s\Gamma c\theta + c\beta s\theta)
\end{aligned}
$$

$$
\begin{aligned}
C_{10} &= r_c c\beta c\Gamma + h_p(s\beta s\theta - c\beta s\Gamma c\theta) \\
C_{11} &= -m_{cr} e_c c\Gamma s\theta \\
C_{12} &= m_{cr} e_c(c\beta c\theta - s\beta s\Gamma s\theta) \\
C_{13} &= \dot{\Gamma}^2(h_p s\Gamma - r_c c\Gamma c\theta) + r_c\dot{\theta}(2\dot{\Gamma}s\Gamma s\theta - \dot{\theta}c\Gamma c\theta) - l\dot{\alpha}^2 c\alpha \\
C_{14} &= l\dot{\alpha}^2 s\alpha - r_c\dot{\theta}^2(c\beta s\theta + s\beta s\Gamma c\theta) - \dot{\beta}^2(r_c c\beta s\theta + r_c s\theta s\Gamma c\theta + h_p s\beta c\Gamma) - \dot{\Gamma}^2(r_c s\beta s\Gamma c\theta + h_p s\beta c\Gamma) \\
&= -2r_c\dot{\theta}\dot{\beta}(s\beta c\theta + c\beta s\Gamma s\theta) + 2\dot{\beta}\dot{\Gamma}(r_c c\beta c\Gamma c\theta - h_p c\beta s\Gamma) - 2r_c\dot{\theta}\dot{\Gamma}s\beta c\Gamma s\theta \\
C_{15} &= I_{c_X}(\dot{\beta}\dot{\Gamma}s\Gamma c\theta + \dot{\beta}\dot{\theta}c\Gamma s\theta - \dot{\Gamma}\dot{\theta}c\theta) + (\dot{\beta}s\Gamma + \dot{\theta})(\dot{\Gamma}c\theta - \dot{\beta}c\Gamma s\theta)(I_{c_Y} - I_{c_Z}) \\
C_{16} &= I_{c_Y}(\dot{\beta}\dot{\theta}c\Gamma c\theta + \dot{\Gamma}\dot{\theta}s\theta - \dot{\beta}\dot{\Gamma}s\Gamma s\theta) + (\dot{\beta}s\Gamma + \dot{\theta})(\dot{\Gamma}s\theta + \dot{\beta}c\Gamma c\theta)(I_{c_{Z0}} - I_{c_X})
\end{aligned}
$$
